

Differentiating physicochemical properties between NDRI and sNRI clinically important for the treatment of ADHD



Panpan Wang^{a,b,c}, Tingting Fu^{a,c}, Xiaoyu Zhang^{a,c}, Fengyuan Yang^{a,c}, Guoxun Zheng^{a,c}, Weiwei Xue^{c,*}, Yuzong Chen^d, Xiaojun Yao^e, Feng Zhu^{a,c,**}

^a Innovative Drug Research and Bioinformatics Group, College of Pharmaceutical Sciences, Zhejiang University, Hangzhou 310058, China

^b College of Chemistry and Pharmaceutical Engineering, Huanghuai University, Zhumadian 463000, China

^c School of Pharmaceutical Sciences and Collaborative Innovation Center for Brain Science, Chongqing University, Chongqing 401331, China

^d Bioinformatics and Drug Design Group, Department of Pharmacy, National University of Singapore, Singapore 117543, Singapore

^e State Key Laboratory of Applied Organic Chemistry, Department of Chemistry, Lanzhou University, Lanzhou 730000, China

ARTICLE INFO

Keywords:

ADHD
Norepinephrine-dopamine reuptake inhibitors
Selective norepinephrine reuptake inhibitors
Molecular dynamics
Binding mode

ABSTRACT

Background: Drugs available for treating attention-deficit hyperactivity disorder (ADHD) are mainly selective norepinephrine (sNRIs) and dual norepinephrine-dopamine (NDRIs) reuptake inhibitors. The major problem of sNRIs lies in their delayed onset of action and partial- or non-responses, which makes NDRIs distinguished in drug efficacy. Understanding of the differential binding modes of these 2 types of drugs to their corresponding targets can give great insights into the discovery of privileged drug-like scaffolds with improved efficacy. So far, no such study has been carried out.

Methods: A combinatorial computational strategy, integrating homology modeling, molecular docking, molecular dynamics (MD) and binding free energy calculation, was employed to analyze the binding modes of 8 clinically important ADHD drugs in their targets.

Results: Binding modes of 2 types of ADHD drugs (sNRIs and NDRIs) in their targets was identified for the first time by MD simulation, and 15 hot spot residues were discovered as crucial for NDRIs' binding in hNET and hDAT. Comparing to sNRIs, a clear reduction in the hydrophobic property of NDRIs' one functional group was observed, and the depth of drugs' aromatic ring stretched into the pocket of both targets was further identified as key contributors to drugs' selectivity.

Conclusions: The hydrophobic property of NDRI ADHD drugs' one functional group contributes to their selectivity when bind hNET and hDAT.

General significance: These results provide insights into NDRI ADHD drugs' binding mechanisms, which could be utilized as structural blueprints for assessing and discovering more efficacious drugs for ADHD therapy.

1. Introduction

Attention-deficit/hyperactivity disorder (ADHD) is a mental condition of the neurodevelopmental type, which severely influences the daily life of 40 million individuals [1–3]. The majority of ADHD patients diagnosed in childhood persists into adulthood [4], which leads to serious problems in communication, emotion and career promotion [5]. Cognitive impairments in ADHD patients are primarily regulated by catecholaminergic signaling in prefrontal cortex (PFC) [6], and attenuation in PFC's neurotransmission of norepinephrine (NE) and dopamine (DA) shows profound effects on the progression of ADHD [7–9]. Besides of PFC, nucleus accumbens and striatum are reported to be

extensively associated with ADHD [10,11], and accumulation of DA in these regions can ameliorate patients' cognitive function [11,12].

Till now, nine drugs (amphetamine, atomoxetine, clonidine, dextroamphetamine, guanfacine, lisdexamfetamine, methylphenidate, dextroamphetamine, and methylphenidate) in total were approved by the U.S. Food and Drug Administration (FDA) for the treatment of ADHD and several others (bupropion, LY2216684, modafinil, reboxetine and viloxazine) were in the clinical trials (<https://clinicaltrials.gov/>). Over three quarters of these drugs exerted their therapeutic effects by targeting human norepinephrine transporter (hNET) in PFC [13–15]. Based on the mechanism of action, these drugs were classified into 2 types: selective norepinephrine reuptake inhibitors (sNRIs) and

* Corresponding author.

** Correspondence to: F. Zhu, Innovative Drug Research and Bioinformatics Group, College of Pharmaceutical Sciences, Zhejiang University, Hangzhou 310058, China.
E-mail addresses: xueww@cqu.edu.cn (W. Xue), zhufeng.ns@gmail.com, zhufeng@zju.edu.cn (F. Zhu).

<http://dx.doi.org/10.1016/j.bbagen.2017.07.022>

Received 30 March 2017; Received in revised form 23 July 2017; Accepted 26 July 2017

Available online 27 July 2017

0304-4165/ © 2017 Elsevier B.V. All rights reserved.

norepinephrine-dopamine reuptake inhibitors (NDRIs) [16–18]. As reported, the major problem of sNRIs was their delayed onset of action and partial- or non-response [19–21]. With the approval of NDRIs targeting both hNET and dopamine transporter (hDAT), this class of drugs were discovered to be able to elevate catecholamines in regions of not only PFC but also nucleus accumbens and striatum [22–24], which ensured their rapid onset of action and substantially enhanced response rate (~75%) for the treatment of ADHD [25].

So far, only a few dual reuptake inhibitors with significant clinical importance for treating ADHD were discovered [26–28]. An understanding of the differential binding modes between sNRIs and NDRIs to their corresponding therapeutic targets could provide insights into the discovery of privileged drug-like scaffold with improved efficacy [29–31]. Structures and site-directed mutagenesis studies demonstrated that both sNRIs and NDRIs bind in the S1 sites of hNET and hDAT [32–34]. Given the absence of the crystallographic structures of hNET and hDAT [32], it was a great challenge to discover novel NDRIs. Currently, rational approaches including computational simulation were used to tune drug selectivity in structure based drug design [35–37]. For example, prediction of protein-ligand binding free energy via molecular dynamics (MD) provided abundant information of ligand binding in various targets [38–40] and mutation induced changes in binding free energy [41–45]. Till now, no comprehensive study on the binding mode of sNRIs and NDRIs in their corresponding targets had been carried out, and it was thus in urgent need to distinguish the drug-target binding mechanism between these two types of drugs.

In this study, a combinatorial computational strategy was employed to explore binding modes of sNRIs and NDRIs (clinically important for ADHD treatment) to their corresponding targets. It was observed that drugs' selectivity primarily came from a specific sub-binding site in the drug binding pocket, and the dual targeting structural features of NDRIs were identified. This study offers valuable insights into the structural requirements for developing dual NE and DA reuptake inhibitors for ADHD treatment.

2. Materials and methods

2.1. Collection of clinically important sNRIs and NDRIs for treating ADHD

In total, 11 NDRIs and sNRIs had been approved or in clinical trial for treating ADHD, which included amphetamine (approved NDRI), atomoxetine (approved sNRI), dexamethylphenidate (approved NDRI), LY2216684 (sNRI in Phase 2/3), dextroamphetamine (approved NDRI), reboxetine (sNRI in Phase 2), bupropion (NDRI in Phase 4), lisdexamfetamine (approved NDRI), methylphenidate (approved NDRI), viloxazine (sNRI in Phase 2) and methamphetamine (approved NDRI). As reported, differentiation of binding modes between clinically important NDRIs and sNRIs (approved or in clinical trial for ADHD) could provide significant insight into the discovery of privileged drug-like scaffold with improved drug efficacy [30,46]. Thus, all those 11 clinically important drugs were selected and studied. Among these drugs, lisdexamfetamine was an inactive prodrug of dextroamphetamine [47]; dextroamphetamine and dexamethylphenidate were D-enantiomers of amphetamine and methylphenidate, respectively. These 3 drugs (lisdexamfetamine, amphetamine and methylphenidate) were thus not repeatedly considered in this work, and only the remaining 8 drugs of clinical importance (Fig. 1A) were collected for studying, including 4 NDRIs (dexamethylphenidate, dextroamphetamine, methamphetamine and bupropion) and 4 sNRIs (atomoxetine, LY2216684, reboxetine and viloxazine). 4 out of these 8 were racemic mixture, and their corresponding enantiomers (dextromethamphetamine for methamphetamine, R-bupropion for bupropion, SS-reboxetine for reboxetine and S-viloxazine for viloxazine) identified as contributing the primary therapeutic efficacy [48–51] were therefore selected for further analysis.

2.2. Homology modeling

Sequence alignment using ClustalW2 [52] (Figs. S1 and S2) showed high sequence identity (> 55%) between targets (hNET and hDAT) and dDAT, especially in their S1 binding sites (69.05% and 78.57% for hNET and hDAT, respectively). Currently, there were many popular tools available for constructing homology model, such as *MODELLER* [53], *PRIME* [54], *SWISS-MODEL* [55], *SYBYL-X* [56], *Insight II* [57] and *MOE* [58]. Based on a comprehensive assessment of the prediction ability of these popular tools [59], *MODELLER* and *SWISS-MODEL* were reported to give “best fold description” as assessed by multiple statistical ranking schemes [59], and *SWISS-MODEL* was also found to be highly accurate and very popular in constructing homology model for target protein of > 50% sequence identity with its corresponding template [59,60]. Thus, *SWISS-MODEL* was selected for constructing the homology models of hNET and hDAT in this study. The corresponding templates were X-ray crystal structures of *Drosophila melanogaster* dopamine transporter (dDAT) complexed with structural similar ligands for studied drugs [29,61] (Table S1 and Fig. S3). The stereochemical quality of the built hNET and hDAT structures were further validated by the Ramachandran plots analysis in the *PROCHECK* [62,63]. The homology models of hNET and hDAT were shown in Fig. 1B.

2.3. Molecular docking

Molecular docking is important and popular for investigating ligand-target interaction, and is applied to associate the spatial orientation of ligand-protein according to their scoring [64]. In this work, initial conformation of each complex for MD simulation was thus obtained by molecular docking using *Glide* [54] with standard precision (SP). Drugs' binding sites in the models of hNET and hDAT were defined by the centroid of corresponding ligands from the template structures (Table S1). The docking poses of these 8 drugs were selected according to the orientations of ligands. Details about the docking protocol were described in **Supplementary Methods**.

2.4. System Setup and MD Simulation

MD simulation is an advanced method presenting precise interaction between ligand and protein at the atomic level by incorporating biological condition such as structural motion [41,64,65]. The resulting docking complexes were thus firstly inserted into POPC bilayers generated by the *Membrane Builder* tool in *CHARMM-GUI* [66], and then solvated with TIP3P water of 20 Å thickness [67]. Finally, each system was neutralized at a salt concentration of 0.15 mol/L, which contained 89,000–99,000 atoms per periodic cell with various box sizes as summarized in **Table S2**.

MD simulations were carried out using *AMBER14* package [68] based on *ff14SB* [69] and *Lipid14* [70] force fields for proteins and lipids respectively by GPU-accelerated *PMEMD* as described in previous work [41,71]. Prior to each simulation, systems underwent a succession of pretreatments including (1) steepest descent minimization, (2) heating to 310 K via 2 sequential stages and (3) 5 ns equilibration at 310 K. Then, 150 ns MD simulation was executed at 310 K and 1 atm in NPT ensemble by the periodic boundary condition. During the simulation, long-range electrostatic interaction (cutoff = 10 Å) was used to evaluate the direct space interactions by *particle-mesh Ewald method* [72], and all bonds involving hydrogen atoms were constrained by *SHAKE algorithm* [73] with 2 fs time step. Finally, 500 snapshots were retrieved from the last 50 ns equilibrium trajectory of each system. More details were extensively described in **Supplementary Methods**.

2.5. Calculation of binding free energy

The total binding free energy ($\Delta G_{\text{calc}}(\text{MM}/\text{GBSA})$) neglected entropic

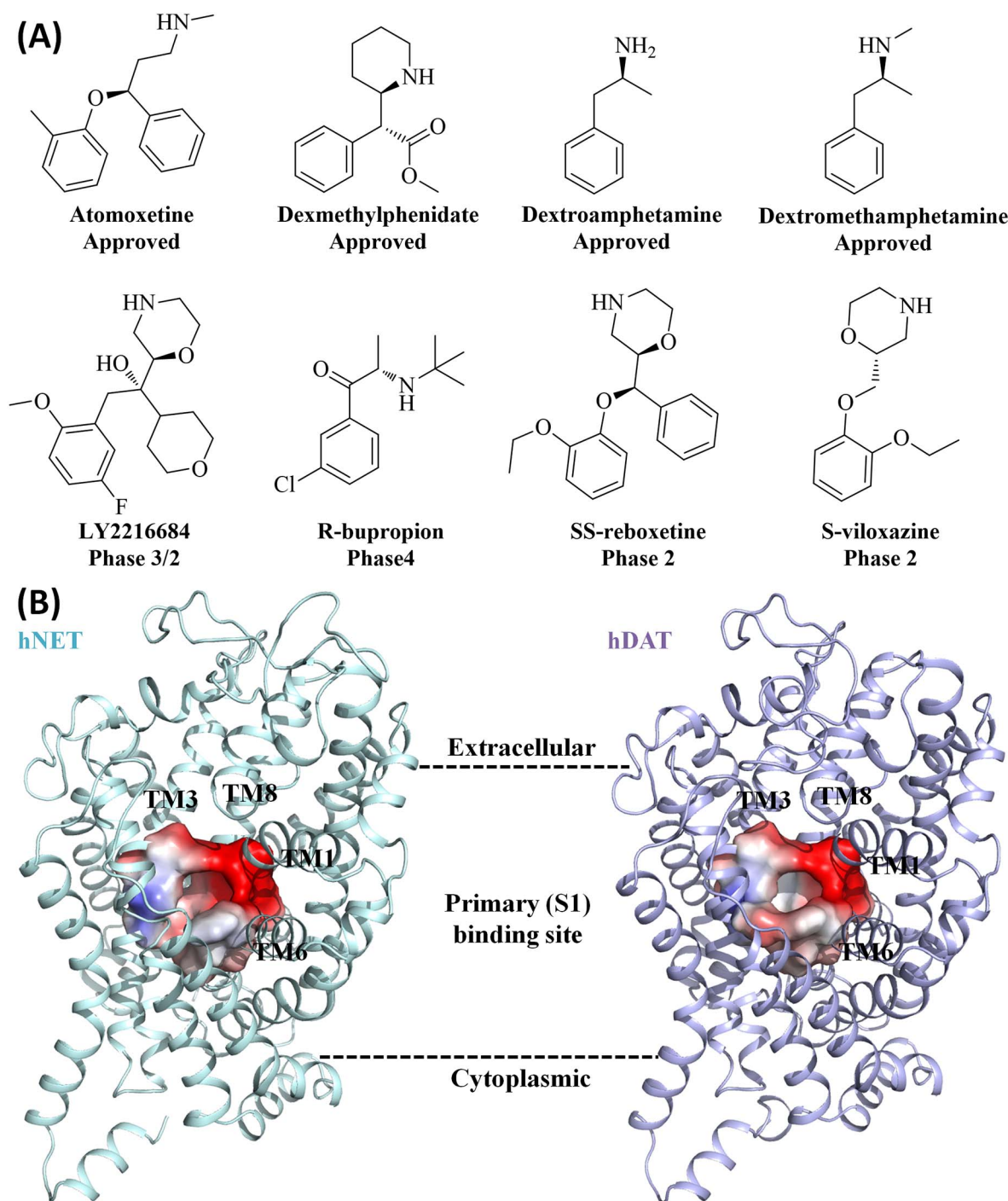


Fig. 1. Structures of 8 ADHD drugs studied in this work (A) and primary (S1) binding sites of hNET and hDAT (B).

contribution of 8 drugs binding to hNET and hDAT were calculated by the MM/GBSA based on 500 snapshots of each single-trajectory [74–77]. For each snapshot, the binding-free energy was obtained by the following equation:

$$\Delta G_{\text{calc}}(\text{MM}/\text{GBSA}) = \Delta E_{\text{vdW}} + \Delta E_{\text{ele}} + \Delta G_{\text{pol}} + \Delta G_{\text{nonpol}} \quad (1)$$

$$\Delta G'_{\text{calc}}(\text{MM}/\text{GBSA}) = \Delta G_{\text{calc}}(\text{MM}/\text{GBSA}) - T\Delta S \quad (2)$$

ΔE_{vdW} and ΔE_{ele} were the Van der Waals interaction and the electrostatic contribution in gas phase, ΔG_{pol} and ΔG_{nonpol} were polar and non-polar contributions to solvation free energy. What needed to be clarified is that ΔG_{nonpol} was received by the surface tension 0.0072 multiplying ΔSASA by linear combination of pairwise overlaps method

(LCPO) with a 1.4 Å Probe radii [78,79]. – $T\Delta S$ referred to the change of conformational entropies upon ligand binding calculating by normal mode analysis [80]. Per-residue decomposition free energy ($\Delta G_{\text{calc}}(\text{MM}/\text{GBSA})^{\text{per-residue}}$) used to quantitatively evaluate every residue contribution to binding was calculated according to the equation:

$$\Delta G_{\text{calc}}(\text{MM}/\text{GBSA})^{\text{per-residue}} = \Delta E_{\text{vdW}}^{\text{per-residue}} + \Delta E_{\text{ele}}^{\text{per-residue}} + \Delta G_{\text{pol}}^{\text{per-residue}} + \Delta G_{\text{nonpol}}^{\text{per-residue}} \quad (3)$$

In Eq. (3), $\Delta E_{\text{vdW}}^{\text{per-residue}}$, $\Delta E_{\text{ele}}^{\text{per-residue}}$ and $\Delta G_{\text{pol}}^{\text{per-residue}}$ were calculated using the same method as that evaluating total binding free energy, and the non-polar solvation free energy contributions were estimated by $\Delta G_{\text{nonpol}}^{\text{per-residue}} = 0.0072 \times \Delta\text{SASA}$. But the SASA was

achieved by icosahedron (ICOSA) only used in the decomposition based on the recursive approximation of a sphere around an atom [81]. Detailed information on the above process was extensively described in **Supplementary Methods**.

2.6. Hierarchical clustering analysis of decomposed per-residue energy contributions

Hierarchical clustering of the contributed residues (contribution $\neq 0$ kcal/mol) was carried out using R statistical analysis software [82,83] according to the similarity degrees among those generated vectors reflected by the *Manhattan distance*:

$$\text{Distance}(a, b) = \sum_{i=1}^l |a_i - b_i| \quad (4)$$

In Eq. (4), l was the dimension of vector, and i was certain residue energy for each dimension. The *Ward's minimum variance method* [84] used in cluster could minimize the total within-cluster variance. Visual hierarchical tree was displayed by online tool *iTOL* [85].

3. Results and discussion

3.1. Homology models of hNET and hDAT

To construct accurate and precise homology models of hNET and hDAT, the X-ray crystal structures of dDAT complexed with diverse ligands were used as templates (**Table S1**). As shown in **Table S1** and **Fig. S2**, all templates adopted in this work showed high sequence identity ($> 55\%$) with hNET or hDAT, especially in S1 binding site (69.05% and 78.57% for hNET and hDAT, respectively). The constructed homology models covered all 12 TMs and the corresponding intervening loops. The detailed sequence range of each model was shown in **Table S1**. Furthermore, the stereochemical quality and accuracy of hNET and hDAT models were further validated by Ramachandran plot (**Fig. S4**). Results showed that residues of models in allowed regions ranged from about 99.6% to 100%, indicating reasonable model conformations [86]. Finally, two functional sodions, one chloridion and two cholesterol or cholesterol with a cholesteryl hemisuccinate in template were fitted into their corresponding binding sites in both hNET and hDAT models.

3.2. Docking the Studied sNRIs and NDRIs into hNET and hDAT

Dextroamphetamine and dextromethamphetamine were reported to be co-crystallized with dDAT [29]. Thus, cross-docking was first carried out to validate the credibility of docking protocol (**Fig. S5**). The binding

pose of dextroamphetamine and dextromethamphetamine obtained by docking was close to the experimentally observed conformation indicated by the valued of root mean square deviation (RMSD were 0.1979 Å and 0.3192 Å, respectively). Then, using the same parameter settings as cross-docking, 4 sNRIs (atomoxetine, LY2216684, SS-reboxetine and S-viloxazine) and 4 NDRIs (dexmethylphenidate, dextroamphetamine, dexmethamphetamine and R-bupropion) were docked into the homology models. Finally, the resulting docking poses of dextroamphetamine and dextromethamphetamine were selected based on their conformations in dDAT (**Fig. S6**), while docking pose of the other 6 drugs was selected according to the orientation of structurally similar ligands co-crystallized with dDAT (**Fig. S7**). **Fig. S8** showed that all drugs bind to the S1 site surrounded by TM1, 3, 6, 8 and 10.

3.3. Assessing the structures of drugs bound hNET and hDAT complexes

3.3.1. Simulation stabilities

After getting the initial poses of those 8 studied drugs in hNET and hDAT, the structures of drug-target complexes were assessed by 150 ns MD simulation in the explicit POPC bilayer membrane. Simulation stabilities were measured by the RMSDs of protein backbone atoms, ligand heavy atoms and binding site residue atoms relative to the initial coordinate of the entire simulation (as illustrated in **Fig. S9**). As shown, all systems reached equilibration around 100 ns and the extending 50 ns trajectory of all systems demonstrated little fluctuation (within 1 Å). Besides LY2216684, RMSDs of hNET's backbone atoms complexed with other drugs were all relatively small (2 Å–3 Å as shown in **Fig. S9A**). A relatively high RMSD (about 6 Å) of hNET's backbone atoms was observed for LY2216684, which might be owing to the extremely flexible EL2 region located far away from the binding pocket (**Fig. S10**). As illustrated, RMSDs of TM1-TM12 were from 0.9430 Å to 1.9660 Å, but RMSD of EL2 equaled to 6.0803 Å, which supported the above extrapolation that higher hNET RMSD of LY2216684 might come from EL2.

3.3.2. Binding free energy analysis

Based on the snapshots extracted from equilibrated trajectories, energies ($\Delta G_{\text{calc}}(\text{MM}/\text{GBSA})$) of ADHD drugs binding to hNET and hDAT were calculated. The calculated $\Delta G_{\text{calc}}(\text{MM}/\text{GBSA})$ and experimental binding affinities (ΔG_{exp}) estimated by reported K_i values [87–94] by $\Delta G_{\text{exp}} = RT \ln(K_i)$ ($R = 8.314 \text{ J}/(\text{K} \cdot \text{mol})$, $T = 310 \text{ K}$) were all summarized in **Table 1**. $\Delta G_{\text{calc}}(\text{MM}/\text{GBSA})$ were overestimated compared to those of experiments. Overestimated binding energies also occurred in other simulations using MM/GBSA method [95–97]. To evaluate whether these overestimation came from the exclusion of entropy contributions,

Table 1

The calculated and experimental binding energies of 8 ADHD drugs binding to wild type hNET and hDAT (ΔG is in kcal/mol and K_i value is in nM).

Drugs ^a	Targets	K_i^b	ΔG_{exp}^c	$\Delta \Delta G_{\text{exp}}^d$	$\Delta G_{\text{calc}}(\text{MM}/\text{GBSA})^e$	$\Delta \Delta G_{\text{calc}}(\text{MM}/\text{GBSA})^d$
AMP	hNET	3820	-7.679	5.053	-33.12 ± 0.10	16.26 ± 0.22
	hDAT	5680	-7.435	5.297	-34.2 ± 0.11	15.18 ± 0.23
MPH	hNET	206	-9.477	3.255	-44.62 ± 0.10	4.76 ± 0.22
	hDAT	161	-9.628	3.104	-44.76 ± 0.10	4.62 ± 0.22
MTA	hNET	4280	-7.609	5.123	-35.41 ± 0.09	13.97 ± 0.21
	hDAT	1850	-8.126	4.606	-38.12 ± 0.09	11.26 ± 0.21
R-bupropion	hNET	6970	-7.309	5.423	-38.90 ± 0.10	10.48 ± 0.22
	hDAT	871	-8.589	4.143	-40.78 ± 0.10	8.60 ± 0.22
Atomoxetine	hNET	5	-11.766	0.966	-48.33 ± 0.12	1.05 ± 0.24
LY2216684	hNET	16	-11.05	1.682	-48.69 ± 0.12	0.69 ± 0.24
SS-reboxetine	hNET	1.04	-12.732	0	-49.38 ± 0.12	0
S-viloxazine	hNET	73	-10.115	2.617	-47.16 ± 0.11	2.22 ± 0.23

^a AMP: dextroamphetamine; MPH: dexmethylphenidate; MTA: dextromethamphetamine.

^b Experimental K_i value from previously published works [87–94].

^c Estimated binding energy based on K_i values using $\Delta G_{\text{exp}} = RT \ln(K_i)$, $R = 8.314 \text{ J}/(\text{K} \cdot \text{mol})$, $T = 310 \text{ K}$.

^d Binding energy difference was computed using $\Delta \Delta G = \Delta G - \Delta G_{\text{SS-reboxetine}}$.

^e Calculated binding energy in this work.

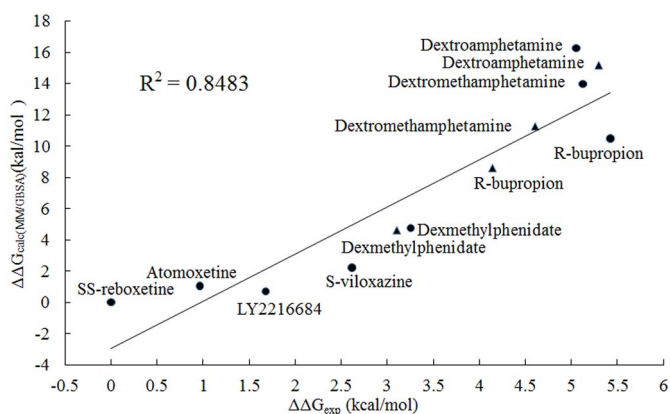


Fig. 2. Graphical representation of correlation between the calculated binding energy differences ($\Delta\Delta G_{\text{calc}}(\text{MM}/\text{GBSA})$) and that of experimental ($\Delta\Delta G_{\text{exp}}$) for 12 studied drugs complexes with the wild type hNET/hDAT. Drugs binding to hNET are represented as black solid dot and Black solid triangle is for hDAT.

– TΔS was calculated by normal mode analysis in this study (Table S3). As a result, the correlation coefficient between $\Delta\Delta G'_{\text{calc}}(\text{MM}/\text{GBSA})$ and $\Delta\Delta G_{\text{exp}}$ equaled to 0.7719 (Fig. S11). This demonstrated good correlation between calculation and experiments but slightly lower than that excluding the entropy contribution (0.8483, Fig. 2), which was consistent with previous work [96]. Overall, a good correlation between $\Delta\Delta G_{\text{calc}}$ and $\Delta\Delta G_{\text{exp}}$ were observed, which indicated that drugs' experimental activities could be effectively reproduced by the calculated binding energies of this study.

3.3.3. Validation of MD simulation

To identify reliable binding modes of studied ADHD drugs in hNET and hDAT, it was indispensable to validate whether the constructed models could accurately reflect real systems or not. Besides the good correlation between the calculated and the experimental binding energies, three lines of evidence were further provided to validate the simulation results of this work.

The first line of evidence was the reproducibility of experimental mutagenesis results [32,98–100] by MD simulated models. A total of 18 site-directed mutational systems were constructed on the basis of wild-type models from MD simulation, and the simulations extending 20 ns were carried out for each system (Fig. S12). The calculated and the experimental energy difference ($\Delta\Delta G$) as well as fold-change (FC) induced by mutations in both targets were shown in Tables 2 and 3, and detail information of energy terms were summarized in Tables S4 and

Table 2

The calculated and experimental changes in binding energies of ADHD drugs for site directed mutagenesis hNET complexes (ΔG is in kcal/mol). Detail information of each energy term can be found in Table S4.

Drug	Mutation sites	Calculated values		Experimental values	
		$\Delta\Delta G_{\text{calc}}(\text{MM}/\text{GBSA})^a$	$\text{FC}_{\text{calc}}(\text{MM}/\text{GBSA})^b$	FC_{exp}^c	$\Delta\Delta G_{\text{exp}}^d$
Atomoxetine	F72A	0.05	1.08	0.78 (0.55–1.14)	– 0.15 (– 0.37–0.08)
	V148I	– 0.7	0.32	0.22 (0.09–0.43)	– 0.93 (– 1.48 ~ – 0.52)
	G149A	0.62	2.74	3.44 (2.36–5.14)	0.76 (0.53–1.01)
	N153S	0.59	2.61	2.33 (1.73–3.29)	0.52 (0.34–0.73)
	F323Y	1.1	5.97	3.89 (2.45–6.14)	0.84 (0.55–1.12)
	S419 T	1.68	15.32	12.67 (8.73–18.86)	1.56 (1.33–1.81)
	A145S-Y151F-I315V-F316C-S420A-A426S	2.04	27.50	27.87 (18.47–40.15)	2.05 (1.80–2.27)
R-bupropion	A145S-Y151F-I315V-F316C-S420A-A426S	– 1.37	0.11	0.09 (0.05–0.15)	– 1.48 (– 1.84 ~ – 1.17)
	SS-reboxetine	A145S-Y151F-I315V-F316C-S420A-A426S	1.28	8.00	10.27 (7.18–14.31)

^a $\Delta\Delta G_{\text{calc}} = \Delta G_{\text{mutation}} - \Delta G_{\text{wild type}}$.

^b Fold-changes of potency ($\text{FC}_{\text{calc}}(\text{MM}/\text{GBSA})$) were derived from $\Delta\Delta G_{\text{calc}}$, the equation $\Delta\Delta G_{\text{calc}} = RT \ln(\text{FC}_{\text{calc}}(\text{MM}/\text{GBSA}))$, $R = 8.314 \text{ J}/(\text{K} \cdot \text{mol})$, $T = 310 \text{ K}$.

^c Fold-changes of potency (FC_{exp}) measured by K_i values ($\text{FC}_{\text{exp}} = K_i(\text{mutation})/K_i(\text{wild type})$) [32,99]. Numbers out of the bracket indicated the fold-changes derived from the mean experimental values of both $K_i(\text{mutation})$ and $K_i(\text{wild type})$. The first number in the bracket indicated the minimum fold-changes, while the second one indicated the maximum fold-changes.

^d $\Delta\Delta G_{\text{exp}}$ were derived from the FC_{exp} by the equation $\Delta\Delta G_{\text{exp}} = RT \ln(\text{FC}_{\text{exp}})$.

S5. As demonstrated in Tables 2 and 3, the $\Delta\Delta G_{\text{calc}}(\text{MM}/\text{GBSA})$ and $\Delta\Delta G_{\text{exp}}$ of all mutational systems were highly consistent with each other, which verified the MD simulated models constructed in this study.

The second line of evidence came from the models' capacity of distinguishing sensitive residues from non-sensitive ones. Drug sensitivity profiles induced by residue mutations could provide great insight into ADHD drugs' binding in hNET and hDAT [99]. Meanwhile, the sensitivity of each residue could be *in silico* estimated by the energy difference between wild-type and mutation system [99]. Herein, 6 mutations S419 T, F323Y, F72A, G149A, N153S and V148I located in hNET S1 site for atomoxetine binding characterized by previous experiments [99] were selected. According to the comparison of FC values between *in silico* studies and experiments (Table 2), the sensitivity profiles of these mutations were successfully reproduced. S419 T and F323Y in hNET were identified here as sensitive mutations ($\text{FC} \geq 5$) for atomoxetine binding. It should be noted that the calculated FC of F323Y for atomoxetine was 5.97, which was within the range of experimental result (2.45–6.14). Meanwhile, F323Y in hNET was also discovered as sensitive mutation for other sNRIs (nisoxetine and maprotiline) [99]. For F72A, G149A, N153S and V148I, the simulations of this work could correctly predict them as non-sensitive mutations ($\text{FC} < 5$). Thus, the *in silico* site-directed mutagenesis study based on the wild-type models constructed by MD simulation could correctly distinguish those sensitive residues from non-sensitive ones. The conformation changes in hNET's binding pocket and shifts of drugs accommodating into the pocket were also illustrated in Fig. S13.

The third evidence lied in the solved co-crystallized structures of amphetamine and methamphetamine complexed with dDAT [29]. Comparison of crystal structures and MD-simulated models revealed the similar binding mode. In details, amino groups of amphetamine and methamphetamine interacted with Asp46 in dDAT (corresponding residues Asp75 in hNET and Asp79 in hDAT) and occupied subsite A lined by Phe43, Ala44, Phe319 and Ser320 (corresponding residues Phe72, Ala73, Phe317 and Ser318 in hNET and Phe76, Ala77, Phe320 and Ser321 in hDAT) [29]. In addition, their phenyl groups were stabilized by inserting into hydrophobic cleft formed by Val120, Tyr124 and Ser422 (corresponding residues Val148, Tyr152 and Ser420 in hNET and Val152, Tyr156 and Ala423 in hDAT) and Phe319 and Phe325 (corresponding residues Phe317 and Phe323 in hNET and Phe320 and Phe326 in hDAT) with van der Waals, which probably played a key role in affinity and especially in specificity owing to non-conserved residues between hDAT and hNET [29,32]. As shown in Fig. 3, all of these mentioned residues were identified as of significant contributors to the binding of those studied drugs.

Table 3

The calculated and experimental changes in binding energies of ADHD drugs for site directed mutagenesis hDAT complexes (ΔG is in kcal/mol). Detail information of each energy term can be found in Table S5.

Drug ^a	Mutation sites	Calculated values		Experimental values	
		$\Delta\Delta G_{\text{calc}}(\text{MM}/\text{GBSA})^b$	$\text{FC}_{\text{calc}}(\text{MM}/\text{GBSA})^c$	FC_{exp}^d	$\Delta\Delta G_{\text{exp}}^e$
AMP	D313N	1.53	12.01	12.71 (10.74–14.95)	1.56 (1.46–1.66)
	W84L	0.47	2.15	2.51 (2.12–2.95)	0.57 (0.46–0.67)
MPH	D313N	− 0.49	0.45	0.54 (0.44–0.67)	− 0.38 (− 0.51 ~ − 0.25)
	W84L	− 0.5	0.44	0.52 (0.38–0.73)	− 0.40 (− 0.60 ~ − 0.19)
MTA	D313N	0.74	3.33	4.27 (3.39–5.41)	0.89 (0.75–1.04)
	W84L	0.74	3.33	3.38 (2.53–4.48)	0.75 (0.57–0.92)
R-Bupropion	D313N	− 0.01	0.98	1.11 (0.98–1.26)	0.06 (− 0.01–0.14)
	W84L	0.47	2.15	2.33 (2.13–2.58)	0.52 (0.47–0.58)
	S149A-F155Y-V318I-C319F-A423S-S429A	− 0.49	0.45	0.47 (0.32–0.67)	− 0.46 (− 0.70 ~ − 0.25)

^a AMP: dextroamphetamine; MPH: dexamethylphenidate; MTA: dextromethamphetamine.
^b $\Delta\Delta G_{\text{calc}}(\text{MM}/\text{GBSA}) = \Delta G_{\text{mutation}} - \Delta G_{\text{wild type}}$.
^c Fold-changes of potency ($\text{FC}_{\text{calc}}(\text{MM}/\text{GBSA})$) were derived from $\Delta\Delta G_{\text{calc}}$ the equation $\Delta\Delta G_{\text{calc}}(\text{MM}/\text{GBSA}) = RT \ln(\text{FC}_{\text{calc}}(\text{MM}/\text{GBSA}))$, $R = 8.314 \text{ J}/(\text{K} \cdot \text{mol})$, $T = 310 \text{ K}$.
^d Fold-changes of potency (FC_{exp}) measured by K_i values ($\text{FC}_{\text{exp}} = K_i(\text{mutation})/K_i(\text{wild type})$) [32,98,100]. Numbers out of the bracket indicated the fold-changes derived from the mean experimental values of both $K_i(\text{mutation})$ and $K_i(\text{wild type})$. The first number in the bracket indicated the minimum fold-changes, while the second one indicated the maximum fold-changes.
^e $\Delta\Delta G_{\text{exp}}$ were derived from the FC_{exp} by the equation $\Delta\Delta G_{\text{exp}} = RT \ln(\text{FC}_{\text{exp}})$.

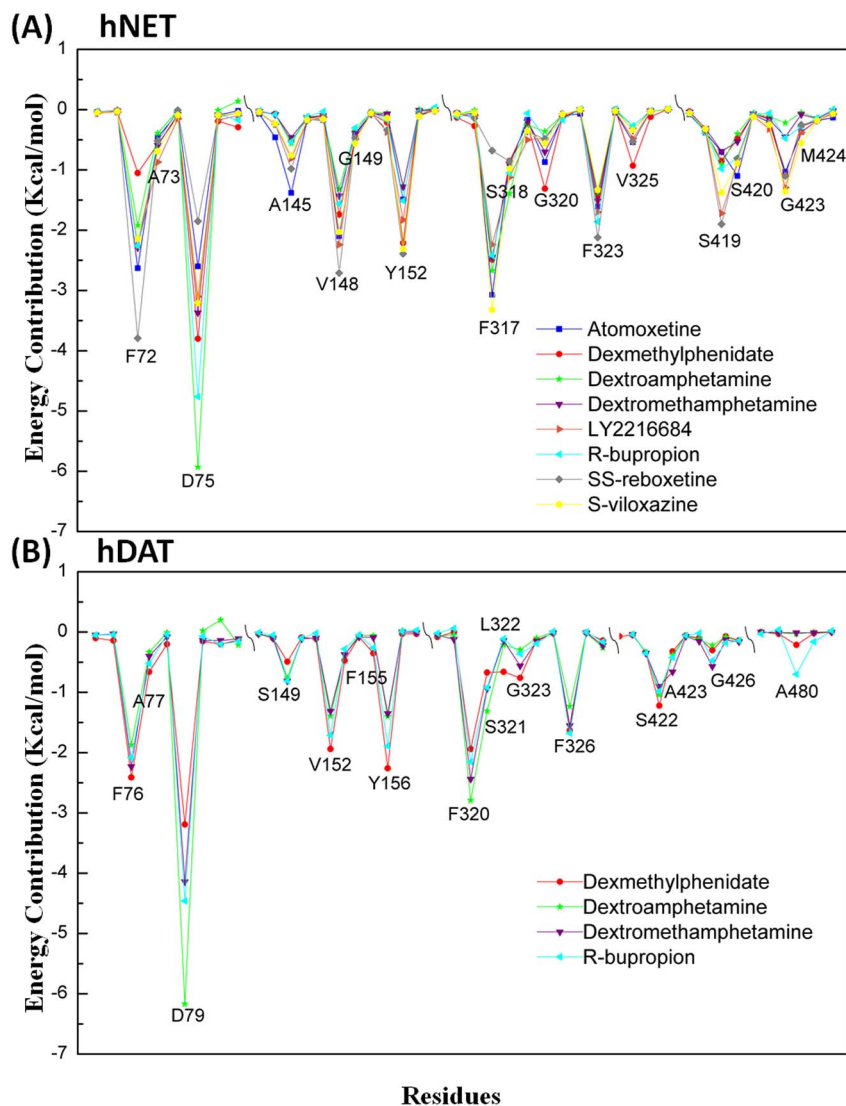


Fig. 3. Per-residue binding free energy decomposition of 12 studied drug-hNET/hDAT complexes. Residues with high energy contribution (the absolute energy contribution ≥ 0.5 kcal/mol) were labeled.

3.4. Identifying the binding modes of the studied sNRIs and NDRIs in hNET and hDAT

3.4.1. Key residues in hNET and hDAT contributing to drugs recognition and binding

The binding mode of 12 complexes was achieved by molecular docking and further identified by MD simulation. Structural alignments of the representative interaction snapshots of 12 studied complexes extracted from equilibrated MD trajectories and their corresponding docking poses were illustrated in Fig. S14. As shown, the conformation of 8 studied ADHD drugs in representative structures extracted from equilibrated simulation trajectory slightly shifted comparing to their corresponding docking poses, and the key interactions such as the salt bridge and hydrogen bond between ligands and Asp75/Asp79 of hNET/hDAT were preserved. Fig. S15 showed the orientations of ADHD drugs and their interacting residues extracted from their corresponding equilibrated MD trajectories. As illustrated, all structures contained the conserved interactions of salt bridge or hydrogen bond between protonated nitrogen ($-N^+$) in drugs' ammonium group and negative charged oxygen (OD^-) of Asp75/Asp79 in hNET/hDAT. The salt bridges between all ADHD drugs and hNET/hDAT were relatively stable in entire MD simulations (Fig. S16). The stability of the hydrogen bonds was estimated by percentage occupancy in each entire trajectory. The occupancy values (ranges from 15.56% to 90.89% as shown in Table S6) demonstrated the stability of hydrogen bonds along each simulation. 7 out of those 8 studied drugs were found to be with high occupancy values, while dextroamphetamine's values were relatively low (15.56 to 18.33%). As shown in Table S6, the low occupancy value of dextroamphetamine in both hNET and hDAT might come from its lower percentage (19.09 to 29.83%) of acceptor...H-donor angles required for hydrogen bond formation [101] compared with that of other studied drugs. In contrast, the salt bridge interaction (Fig. S16C, J) between dextroamphetamine and those two targets were more stable during the entire MD simulations than that of other studied drugs, which was consistent with previous report [29] that the conserved interactions of salt bridge or hydrogen bond were essential for drugs recognition of hNET and hDAT.

In addition, energy contribution of each residue to drugs binding in hNET or hDAT were quantitatively analyzed and illustrated in Fig. 3. To the best of our knowledge, Fig. 3 was the first illustration of the per-residue energy contributions between ADHD drugs and their corresponding targets. There were 14, 13, 9, 11, 11, 13, 14 and 15 residues in hNET with great energy contributions (≥ 0.5 kcal/mol) to the accommodating of atomoxetine, dexamethylphenidate, dextroamphetamine, dextromethamphetamine, R-bupropion, LY2216684, SS-reboxetine and S-viloxazine, respectively (Fig. 3A). Moreover, 11, 9, 12 and 11 residues were considered as the high contribution ones for the binding of dexamethylphenidate, dextroamphetamine, dextromethamphetamine and R-bupropion in hDAT (Fig. 3B). It was noted that, in each complex, energy contributions of the identified high contribution residues varied significantly. For instance, energy contribution to dextroamphetamine's binding varied from -0.56 (-0.76) kcal/mol for Ala145 in hNET (Ser149 in hDAT) to -5.93 (-6.17) kcal/mol for Asp75 in hNET (Asp79 in hDAT). Meanwhile, energy contribution of the same residue in different complex was also different. For example, contributions of Asp75 in hNET varied from -5.93 kcal/mol for dextroamphetamine's binding to -1.85 kcal/mol for SS-reboxetine's binding, and the contribution of Asp79 in hDAT was from -6.17 kcal/mol (dextroamphetamine) to -3.19 kcal/mol (dexamethylphenidate).

3.4.2. The shared binding mode of studied NDRIs in hNET and hDAT

Fig. 3 implied some level of similarity among drugs' binding in both hNET and hDAT, which inspired us to further explore their shared binding mode to facilitate the discovery of new NDRI treating ADHD [30,102]. As shown in Fig. 4, five congregated residue groups (A, B, C,

D and E) were discovered by hierarchical clustering analysis of per-residue energies of 4 studied NDRIs binding to hNET and hDAT. Per-residue binding free energies favoring drugs' binding were colored in red, with the highest energy (-6.17 kcal/mol) set as exact red and the lower energies gradually fading towards white (0 kcal/mol). Per-residue energies hampering drugs' binding were shown in blue, with the highest (0.37 kcal/mol) set as exact blue and lower ones gradually fading towards white (0 kcal/mol). Energy contributions of the residues in group A (Phe72, Asp75, Val148, Tyr152, Phe317, Ser318, Phe323 and Ser419 in hNET, and Phe76, Asp79, Val152, Tyr156, Phe320, Ser321, Phe326 and Ser422 in hDAT) were significantly higher than those in group B, C, D and E. The sum of energy contributions of group A were considered as the primary contributor to NDRIs' binding, consisting of 58.39%, 75.69%, 67.04%, 69.88% energy contribution in hNET, and 65.89%, 78.29%, 69.64%, 70.88% energy contribution in hDAT for binding dexamethylphenidate, dextroamphetamine, dextromethamphetamine, R-bupropion, respectively. Those residues in group B (Ala73, Ala145, Gly149, Gly320, Val325, Asp418, Ser420 and Gly423 in hNET, and Ala77, Ser149, Gly153, Gly323, Asp421, Ala423 and Gly426 in hDAT) offered relatively strong contributions to NDRIs' binding, with 23.18%, 13.04%, 18.14%, 15.98% energy contribution in hNET, and 14.42%, 12.24%, 17.18%, 14.34% energy contribution in hDAT for binding dexamethylphenidate, dextroamphetamine, dextromethamphetamine, R-bupropion, respectively. Taken together, a total of 15 residues in hNET (hDAT) were identified as hot spots in NDRIs' binding.

Fig. 5 illustrated the interaction of 4 studied NDRIs with 15 hot spot residues of hNET and hDAT. As shown, all studied drugs displayed resemble orientation in binding pocket with slight conformational shift. Thus the generalized binding mode of 4 studied NDRIs in hNET/hDAT was schematically shown in Fig. S17. It was clear to observe that 3 chemical moieties of ADHD drug contacted with residues in the binding pocket via both electrostatic and hydrophobic interactions. These chemical moieties were highlighted by light gray (R_1), deep gray (R_2) and gray (R_3), and residues were distinguished by black and gray color on the basis of strong (group A) and relatively strong (group B) energy contribution. In particular, the ammonium moiety R_1 mainly contacted with Asp75 (Asp79) and/or Phe72 (Phe76) and Phe317 (Phe320) in hNET (hDAT) via electrostatic interactions, and R_1 contacted with Ala73 (Ala77) and/or Phe72 (Phe76) in hNET (hDAT) via hydrophobic interactions. As shown in Fig. S17, aromatic moiety R_2 was anchored by hydrophobic interactions in the hydrophobic cleft of hNET (hDAT), while moiety R_3 was surrounded by hydrophobic interactions in another hydrophobic cleft of hNET (hDAT). The studied 4 sNRIs also shared a common binding mode which was consistent with previous studies [71], the detailed information could be found in **Supplementary Results and Discussion**.

3.5. Identification of key physicochemical properties discriminating NDRIs from sNRIs

The homology models of hNET and hDAT shared a similar molecular architecture (Fig. 1B), and their amino acid sequence share an overall identity of $\sim 54\%$ (Fig. S1) and a high identity of 89% in the drug binding site [29]. As reported, the selectivity determinants in hNET were critical for the development of ADHD drug [32,103,104]. Although mutagenesis [29,32,105], crystallography [29] and molecular modeling [103,106] of ADHD drugs were studied, their selectivity determinants were still elusive.

In this study, to make a better understanding of ADHD drugs' selectivity, additional MD simulation of the selective dopamine transporter inhibitor (sDRI) R-modafinil binding to hDAT was performed. The per-residue energies contributing to NDRI's binding and that contributing to sNRI and sDRI's binding were compared by energy variation analysis. Herein, the energy variation was calculated based on the mean energy contribution of residues in S1 sites of both hNET and hDAT (Fig.

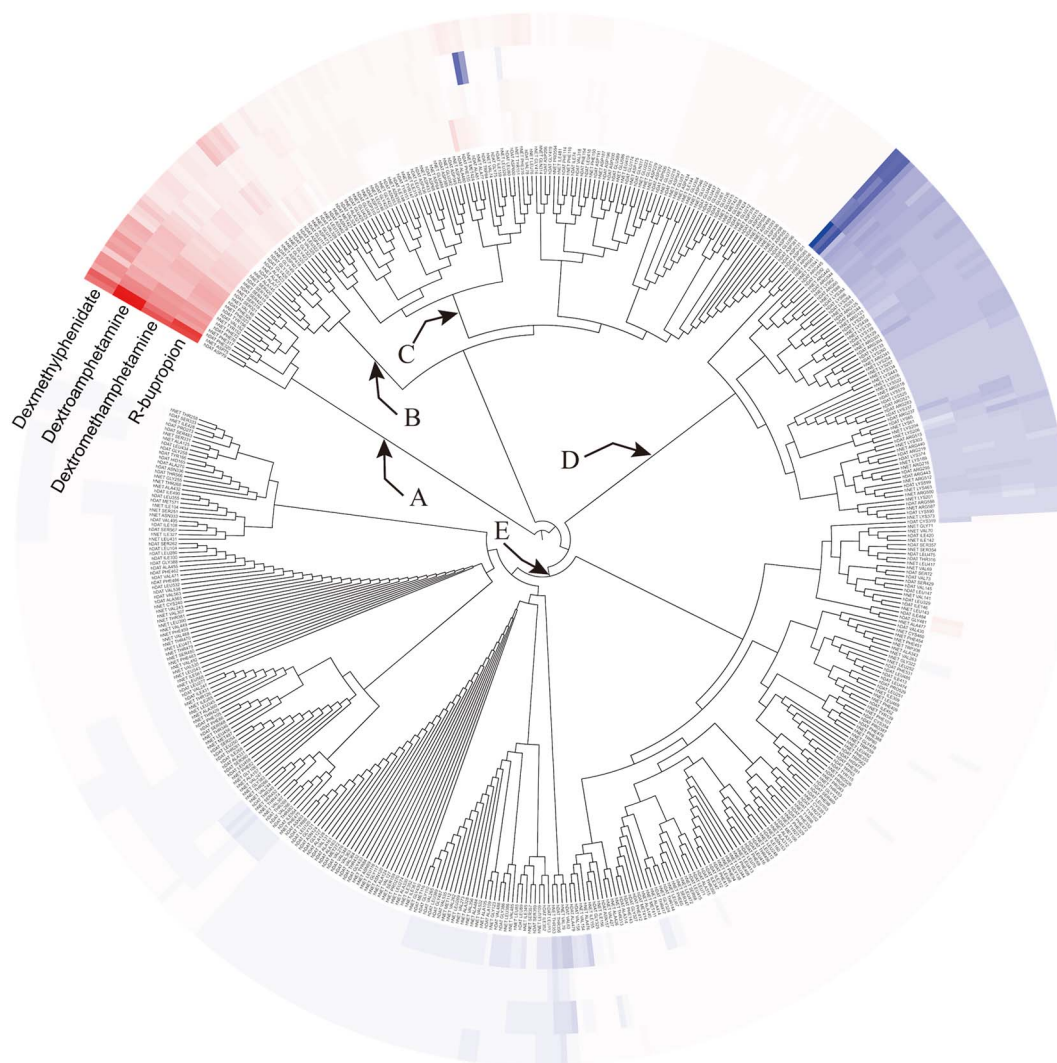


Fig. 4. Hierarchical clustering tree of 492 residues with contributions to at least one complex studied 4 NDRI ADHD drugs in hNET and hDAT binding respectively based on their per-residue energy contributions. Per-residue binding energy contributions favoring ligand's binding were displayed in red, with the highest contribution set as exact red and lower contributions gradually fading towards white (no contribution). Per-residue energy contributions hampering ligand's binding were shown in blue, with the highest one set as exact blue and lower ones gradually fading towards white.

S18A, B). As illustrated, Phe72, Asp75, Ala145, Val148, Tyr152, Ser419, Ser420, Gly423 and Ile481 of hNET and Phe76, Asp79, Val152, Phe155 and Phe320 of hDAT were the key determinants of sNRIs' and sDRIs' selectivity, respectively. Per-residue energy variation of these determinants was summarized in [Tables 4 and 5](#). Schematic representation of the binding mode between those studied drugs and selective determinants in both targets was shown in [Fig. 6](#). Comparing to selective ADHD drugs, hydrophobic interactions in subsite B between residues and R_2 significantly decreased (shown in red) for dual target drugs, which indicated a clear reduction in hydrophobic property of the functional group R_2 in NDRI. This result was further supported by weaker hydrophobic property in R_2 of most NDRI drugs (phenyl group) than that of sNRI drugs (ethoxy-, methoxy- and methyl-substituted phenyl group). Moreover, as an indirect experimental support to this finding, the improved selectivity of SS-reboxetine to hNET [32] could be reflected by the significant increase of hydrophobicity in its R_2 group (ethoxy-phenyl group) comparing to that of nisoxetine (methoxy-phenyl group). Similarly, the hydrophobic interactions of R_3 in NDRI drugs were reduced in subsite C. In the meantime, MD simulation also revealed that residues Asp75 (hNET) and Asp79 (hDAT) played key role in the recognition of all studied drugs. Therefore, as a prerequisite, their corresponding interactions with targets must be preserved in ADHD

drugs' binding. The structural variation in those studied drugs could also induce changes in interaction between R_1 and surrounding residues (Ala77 and Phe320).

Apart from the variations in hydrophobic property as identified above, the selectivity of ADHD drugs could be further reflected by distances among the centroids of R_1 , R_2 and R_3 in each drug. As shown in [Table S7](#), D_1 of NDRI was in the range of 5.18–5.41 Å, which was shorter than that of sNRIs (6.33–8.34 Å), and the range of D_2 for NDRI was from 2.11 Å to 3.81 Å, which was also significantly shorter than that of sNRIs (4.25–6.68 Å). Distance among centroids of ADHD drugs' moieties (R_1 , R_2 and R_3) reflected the depth of the aromatic ring stretched into the hydrophobic pocket, which might be another key physicochemical property for ADHD drugs' selectivity.

4. Conclusions

The common binding mode in targets shared by NDRI for the treatment of ADHD was identified for the first time in this study, and 15 hot spot residues were considered as crucial for the binding NDRI in both targets. Comparing to selective ADHD drugs, a clear reduction in hydrophobic property of the functional group R_2 in NDRI was observed, and the depth of the aromatic ring in drugs stretched into the

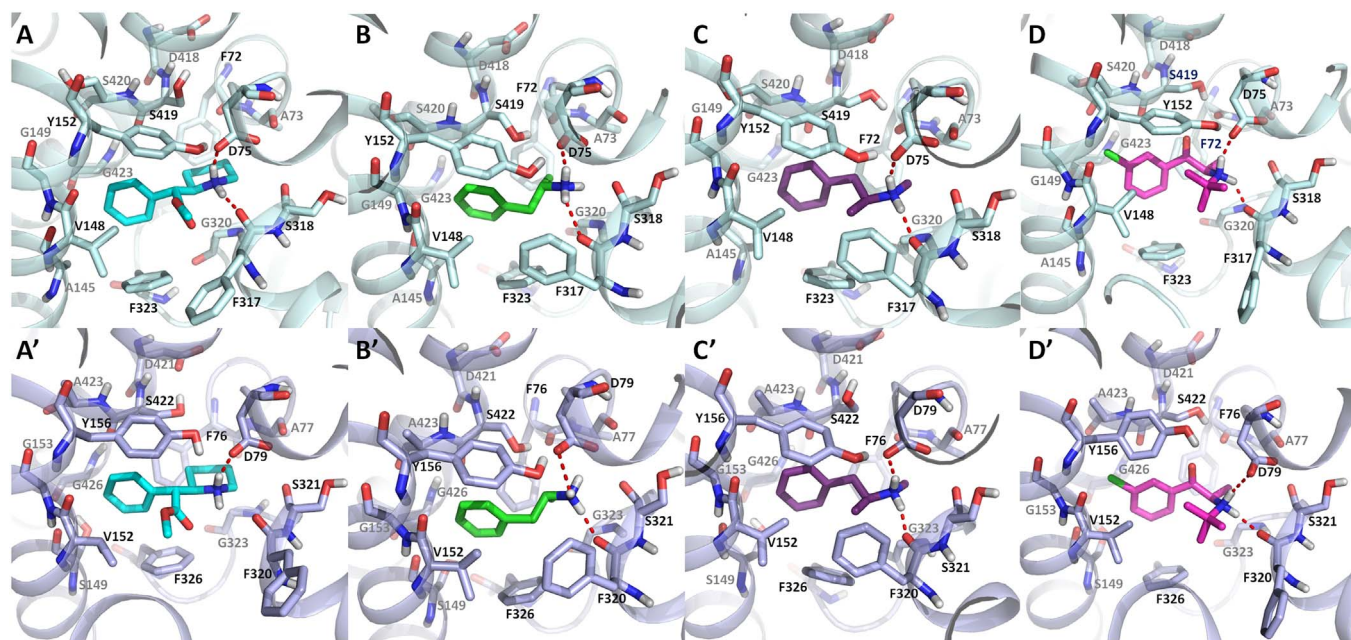


Fig. 5. Proposed binding modes of 4 NDRIs ADHD drugs in 15 hot spot residues of hNET and hDAT. A-D and A'-D' were binding modes of dual-target drugs dexmethylphenidate (cyan), dextroamphetamine (green), dextromethamphetamine (violet), R-bupropion (magenta) in hNET and hDAT. Palecyan and Slateblue cartoon representation was used for the backbone atoms of hNET and hDAT. Residues and ligands were shown in stick representation, and only polar hydrogen atoms are displayed for clarity. Salt bridges and hydrogen bonds are depicted as red dotted lines. Hot residues were distinguished by black and gray color on basis of strong (group A) and relatively strong (group B) contributions respectively (as shown in Fig. 4).

Table 4
Energy contributions of residues in hNET binding site and energy fold changes in each residue between NDRIs and sNRIs.

Residue	NDRIs ^a				sNRIs				EnergyVariation ^b
	MPH	AMP	MTA	R-bupropion	Atomoxetine	LY2216684	SS-reboxetine	S-viloxazine	
PHE72	-1.05	-1.92	-2.29	-2.26	-2.63	-2.26	-3.79	-2.14	0.825
ASP75	-3.8	-5.93	-3.37	-4.76	-2.6	-3.1	-1.85	-3.21	-1.775
ALA145	-0.51	-0.56	-0.46	-0.53	-1.38	-0.81	-0.98	-0.76	0.468
VAL148	-1.74	-1.31	-1.43	-1.56	-2.1	-2.24	-2.71	-2.03	0.760
TYR151	-0.21	-0.06	-0.07	-0.17	-0.11	-0.37	-0.34	-0.14	0.113
TYR152	-2.21	-1.27	-1.28	-1.51	-1.49	-1.83	-2.39	-2.31	0.438
PHE317	-2.49	-2.67	-2.45	-2.42	-3.07	-2.24	-0.68	-3.32	-0.180
SER419	-0.85	-0.91	-0.69	-0.98	-0.7	-1.72	-1.9	-1.38	0.568
SER420	-0.48	-0.4	-0.53	-0.8	-1.1	-0.9	-0.81	-0.89	0.373
GLY423	-1.09	-0.22	-0.45	-0.47	-1.03	-1.29	-1.1	-1.36	0.638
ILE481	-0.06	-0.03	-0.04	-0.06	-0.57	-0.27	-0.69	-0.09	0.358

^a AMP: dextroamphetamine; MPH: dexmethylphenidate; MTA: dextromethamphetamine.

^b The energy variations of per-residue between NDRIs and sNRIs were calculated by Energy Variation = mean energy contribution_{NDRIs} - mean energy contribution_{sNRIs}. Energy Variation is in kcal/mol.

Table 5
Energy contributions of residues in hDAT binding site and energy fold changes in each residue between NDRIs and sDRIs.

Residue	NDRIs ^a				sDRIs	EnergyVariation ^b
	MPH	AMP	MTA	R-bupropion	R-modafinil	
PHE76	-2.41	-1.87	-2.23	-2.08	-2.63	0.483
ASP79	-3.19	-6.17	-4.14	-4.46	-1.48	-3.01
Ser149	-0.49	-0.76	-0.81	-0.81	-0.47	-0.248
VAL152	-1.94	-1.39	-1.31	-1.71	-2.25	0.663
PHE155	-0.35	-0.06	-0.09	-0.26	-0.50	0.310
TYR156	-2.26	-1.4	-1.35	-1.89	-2.02	0.295
PHE320	-1.94	-2.79	-2.44	-2.15	-1.4	-0.93
SER422	-1.22	-1.04	-0.9	-0.98	-1.01	-0.025
ALA423	-0.32	-0.38	-0.66	-0.42	-0.48	0.035
GLY426	-0.3	-0.22	-0.57	-0.47	-0.41	0.02
ILE484	-0.01	0	-0.05	-0.29	-0.21	0.123

^a AMP: dextroamphetamine; MPH: dexmethylphenidate; MTA: dextromethamphetamine.

^b The energy variations of per-residue between NDRIs and sDRIs were calculated by Energy Variation = mean energy contribution_{NDRIs} - mean energy contribution_{sDRIs}. Energy Variation is in kcal/mol.

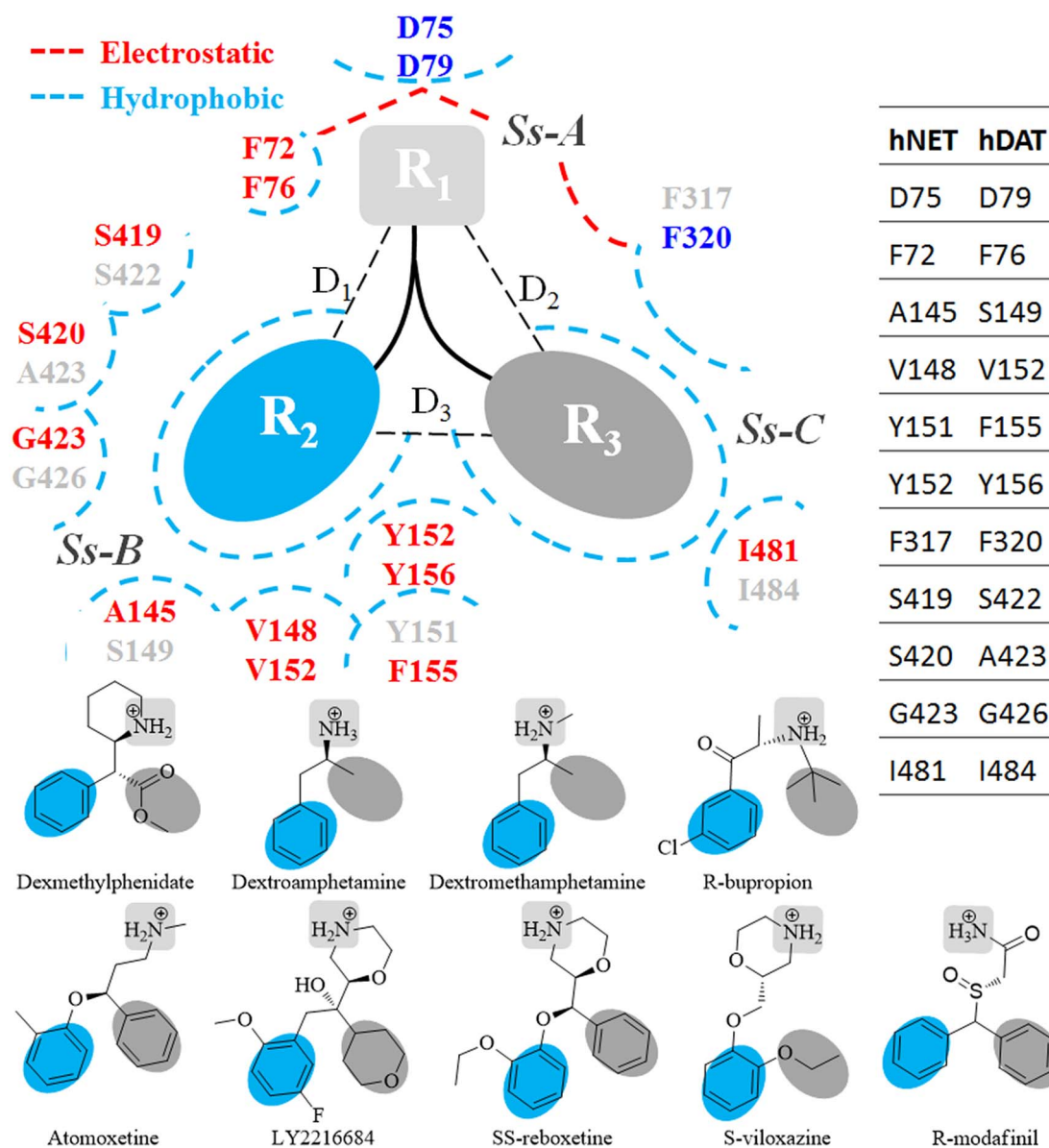


Fig. 6. Schematic representation of the binding mode between studied ADHD drugs and identified selectivity sensitive residues in hNET and/or hDAT. The electrostatic and hydrophobic interactions were depicted in red and light blue dashed lines respectively. *Ss-A*, *Ss-B* and *Ss-C* were subsite A, subsite B and subsite C respectively. R_1 (light gray) were ammonium group with electrostatic interaction to residues in the vicinity, and R_2 (light blue) and R_3 (gray) were aromatic moieties with only hydrophobic interaction to its nearby residues. D_1 , D_2 and D_3 represent distances between the centroid of each drug with its R_1 , R_2 and R_3 groups, respectively. Moreover, Residues contributed more energy to sNRIs' and sDRIs' binding in hNET/hDAT were set red, and ones contributed more energy to NDRIs' binding in targets were set blue. Residues identified as without sensitive in only one target were set as light gray. Additionally groups of R_1 , R_2 and R_3 for each drug were marked by light gray solid rectangular, deep gray and gray solid ellipse respectively at the bottom.

hydrophobic pocket was identified as one of the key contributors to the selectivity of ADHD drugs. These results provide new insights into the binding mechanism of NDRIs clinically important for the treatment of ADHD, which could be further utilized as structural and energetic blueprints for assessing and discovering novel therapeutics for ADHD treatment.

Conflict of interests

The authors declare that they have no conflict of interests.

Transparency Document

The Transparency document associated with this article can be found, in online version.

Funding

This work was supported by National Natural Science Foundation of China [grant number: 21505009]; the Precision Medicine Project of the National Key Research and Development Plan of China [grant number: 2016YFC0902200]; Innovation Project on Industrial Generic Key Technologies of Chongqing [grant number: cstc2015zdcy-ztx120003]; and Fundamental Research Funds for Central Universities [grant number: 10611CDJXZ238826, CDJZR14468801, CDJKXB14011].

Appendix A. Supplementary data

Supplementary data to this article can be found online at <http://dx.doi.org/10.1016/j.bbagen.2017.07.022>.

References

- [1] B. Franke, A.A. Vasquez, S. Johansson, M. Hoogman, J. Romanos, A. Boreatti-Hummer, M. Heine, C.P. Jacob, K.P. Lesch, M. Casas, M. Ribases, R. Bosch, C. Sanchez-Mora, N. Gomez-Barros, N. Fernandez-Castillo, M. Bayes, A. Halmoy, H. Halleland, E.T. Landaas, O.B. Fasmer, P.M. Knappskog, A.J. Heister, L.A. Kiemeny, J.J. Kooij, A.M. Boonstra, C.C. Kan, P. Asherson, S.V. Faraone, J.K. Buitelaar, J. Haavik, B. Cormand, J.A. Ramos-Quiroga, A. Reif, Multicenter analysis of the SLC6A3/DAT1 VNTR haplotype in persistent ADHD suggests differential involvement of the gene in childhood and persistent ADHD, *Neuropsychopharmacology* 35 (2010) 656–664.
- [2] C. Global Burden of Disease Study, Global, regional, and national incidence, prevalence, and years lived with disability for 301 acute and chronic diseases and injuries in 188 countries, 1990–2013: a systematic analysis for the global burden of disease study 2013, *Lancet* 386 (2015) 743–800.
- [3] P. Wang, X. Zhang, T. Fu, S. Li, B. Li, W. Xue, X.J. Yao, Y. Chen, F. Zhu, Differentiating physicochemical properties between addictive and nonaddictive adhd drugs revealed by molecular dynamics simulation studies, *ACS Chem. Neurosci.* 8 (2017) 1416–1428.
- [4] L. Garcia Murillo, M.A. Ramos-Olagazasti, S. Mannuzza, F.X. Castellanos, R.G. Klein, Childhood attention-deficit/hyperactivity disorder and homelessness: a 33-year follow-up study, *J. Am. Acad. Child Adolesc. Psychiatry* 55 (2016) 931–936.
- [5] T.V. Maia, M.J. Frank, From reinforcement learning models to psychiatric and neurological disorders, *Nat. Neurosci.* 14 (2011) 154–162.
- [6] J.M. Drerup, K. Hayashi, H. Cui, G.L. Mettlach, M.A. Long, M. Marvin, X. Sun, M.S. Goldberg, M. Lutter, J.A. Bibb, Attention-deficit/hyperactivity phenotype in mice lacking the cyclin-dependent kinase 5 cofactor p35, *Biol. Psychiatry* 68 (2010) 1163–1171.
- [7] T.J. Brozoski, R.M. Brown, H.E. Rosvold, P.S. Goldman, Cognitive deficit caused by regional depletion of dopamine in prefrontal cortex of rhesus monkey, *Science* 205 (1979) 929–932.
- [8] A.F. Arnsten, B.M. Li, Neurobiology of executive functions: catecholamine influences on prefrontal cortical functions, *Biol. Psychiatry* 57 (2005) 1377–1384.
- [9] F. Zhu, Z. Shi, C. Qin, L. Tao, X. Liu, F. Xu, L. Zhang, Y. Song, X. Liu, J. Zhang, B. Han, P. Zhang, Y. Chen, Therapeutic target database update 2012: a resource for facilitating target-oriented drug discovery, *Nucleic Acids Res.* 40 (2012) D1128–D1136.
- [10] B. Li, J. Tang, Q. Yang, X. Cui, S. Li, S. Chen, Q. Cao, W. Xue, N. Chen, F. Zhu, Performance evaluation and online realization of data-driven normalization methods used in LC/MS based untargeted metabolomics analysis, *Sci. Rep.* 6 (2016) 38881.
- [11] F.X. Castellanos, R. Tannock, Neuroscience of attention-deficit/hyperactivity disorder: the search for endophenotypes, *Nat. Rev. Neurosci.* 3 (2002) 617–628.
- [12] Y.H. Li, P.P. Wang, X.X. Li, C.Y. Yu, H. Yang, J. Zhou, W.W. Xue, J. Tan, F. Zhu, The human kinome targeted by fda approved multi-target drugs and combination products: a comparative study from the drug-target interaction network perspective, *PLoS One* 11 (2016) e0165737.
- [13] T. Vanicek, M. Spies, C. Rami-Mark, M. Savli, A. Hoflich, G.S. Kranz, A. Hahn, A. Kutzelnigg, T. Traub-Weidinger, M. Mitterhauser, W. Wadsak, M. Hacker, N.D. Volkow, S. Kasper, R. Lanzenberger, The norepinephrine transporter in attention-deficit/hyperactivity disorder investigated with positron emission tomography, *JAMA Psychiat.* 71 (2014) 1340–1349.
- [14] J. Xu, P. Wang, H. Yang, J. Zhou, Y. Li, X. Li, W. Xue, C. Yu, Y. Tian, F. Zhu, Comparison of FDA approved kinase targets to clinical trial ones: insights from their system profiles and drug-target interaction networks, *Biomed. Res. Int.* 2016 (2016) 2509385.
- [15] Y.H. Li, J.Y. Xu, L. Tao, X.F. Li, S. Li, X. Zeng, S.Y. Chen, P. Zhang, C. Qin, C. Zhang, Z. Chen, F. Zhu, Y.Z. Chen, SVM-Prot 2016: A web-server for machine learning prediction of protein functional families from sequence irrespective of similarity, *PLoS One* 11 (2016) e0155290.
- [16] B. Dell'Osso, M.C. Palazzo, L. Oldani, A.C. Altamura, The noradrenergic action in antidepressant treatments: pharmacological and clinical aspects, *CNS Neurosci. Ther.* 17 (2011) 723–732.
- [17] H. Yang, C. Qin, Y.H. Li, L. Tao, J. Zhou, C.Y. Yu, F. Xu, Z. Chen, F. Zhu, Y.Z. Chen, Therapeutic target database update 2016: enriched resource for bench to clinical drug target and targeted pathway information, *Nucleic Acids Res.* 44 (2016) D1069–D1074.
- [18] B. Li, J. Tang, Q. Yang, S. Li, X. Cui, Y. Li, Y. Chen, W. Xue, X. Li, F. Zhu, NOREVA: normalization and evaluation of MS-based metabolomics data, *Nucleic Acids Res.* 45 (2017) W162–W170.
- [19] F.P. Bymaster, K. Golembiowska, M. Kowalska, Y.K. Choi, F.I. Tarazi, Pharmacological characterization of the norepinephrine and dopamine reuptake inhibitor EB-1020: implications for treatment of attention-deficit hyperactivity disorder, *Synapse* 66 (2012) 522–532.
- [20] L. Briars, T. Todd, A review of pharmacological management of attention-deficit/hyperactivity disorder, *J. Pediatr. Pharmacol. Ther.* 21 (2016) 192–206.
- [21] S. Cortese, M. Holtmann, T. Banaschewski, J. Buitelaar, D. Coghill, M. Danckaerts, R.W. Dittmann, J. Graham, E. Taylor, J. Sergeant, A.G.G. European, Practitioner review: current best practice in the management of adverse events during treatment with ADHD medications in children and adolescents, *J. Child Psychol. Psychiatry* 54 (2013) 227–246.
- [22] Z. Freyberg, M.S. Sonders, J.J. Aguilar, T. Hiranita, C.S. Karam, J. Flores, A.B. Pizzo, Y. Zhang, Z.J. Farino, A. Chen, C.A. Martin, T.A. Kojajic, H. Fei, G. Hu, Y.Y. Lin, E.V. Mosharov, B.D. McCabe, R. Freyberg, K. Wimalasena, L.W. Hsin, D. Sames, D.E. Krantz, J.L. Katz, D. Sulzer, J.A. Javitch, Mechanisms of amphetamine action illuminated through optical monitoring of dopamine synaptic vesicles in *Drosophila* brain, *Nat. Commun.* 7 (2016) 10652.
- [23] J. Cheng, Z. Xiong, L.J. Duffney, J. Wei, A. Liu, S. Liu, G.J. Chen, Z. Yan, Methylphenidate exerts dose-dependent effects on glutamate receptors and behaviors, *Biol. Psychiatry* 76 (2014) 953–962.
- [24] F. Zhu, L. Han, C. Zheng, B. Xie, M.T. Tammi, S. Yang, Y. Wei, Y. Chen, What are next generation innovative therapeutic targets? Clues from genetic, structural, physicochemical, and systems profiles of successful targets, *J. Pharmacol. Exp. Ther.* 330 (2009) 304–315.
- [25] T. Spencer, J. Biederman, T. Wilens, R. Doyle, C. Surman, J. Prince, E. Mick, M. Aleardi, K. Herzig, S. Faraone, A large, double-blind, randomized clinical trial of methylphenidate in the treatment of adults with attention-deficit/hyperactivity disorder, *Biol. Psychiatry* 57 (2005) 456–463.
- [26] S. Santra, H. Sharma, S. Vedachalam, T. Antonio, M. Reith, A. Dutta, Development of potent dopamine-norepinephrine uptake inhibitors (DNRIIs) based on a (2S,4R,5R)-2-benzhydryl-5-((4-methoxybenzyl)amino)tetrahydro-2H-pyran-4-ol molecular template, *Bioorg. Med. Chem.* 23 (2015) 821–828.
- [27] S. Paudel, S. Acharya, G. Yoon, K.M. Kim, S.H. Cheon, Exploration of substituted arylpiperazine-tetrazoles as promising dual norepinephrine and dopamine reuptake inhibitors, *Bioorg. Med. Chem.* 24 (2016) 5546–5555.
- [28] F. Zhu, B. Han, P. Kumar, X. Liu, X. Ma, X. Wei, L. Huang, Y. Guo, L. Han, C. Zheng, Y. Chen, Update of TTD: therapeutic target database, *Nucleic Acids Res.* 38 (2010) D787–D791.
- [29] K.H. Wang, A. Penmatsa, E. Gouaux, Neurotransmitter and psychostimulant recognition by the dopamine transporter, *Nature* 521 (2015) 322–327.
- [30] A. Yan, L. Wang, S. Xu, J. Xu, Aurora-A kinase inhibitor scaffolds and binding modes, *Drug Discov. Today* 16 (2011) 260–269.
- [31] L. Tao, F. Zhu, F. Xu, Z. Chen, Y.Y. Jiang, Y.Z. Chen, Co-targeting cancer drug escape pathways confers clinical advantage for multi-target anticancer drugs, *Pharmacol. Res.* 102 (2015) 123–131.
- [32] J. Andersen, K.B. Ringsted, B. Bang-Andersen, K. Stromgaard, A.S. Kristensen, Binding site residues control inhibitor selectivity in the human norepinephrine transporter but not in the human dopamine transporter, *Sci. Rep.* 5 (2015) 15650.
- [33] A. Penmatsa, K.H. Wang, E. Gouaux, X-ray structures of *Drosophila* dopamine transporter in complex with nisoxetine and roboxetine, *Nat. Struct. Mol. Biol.* 22 (2015) 506–508.
- [34] L. Tao, F. Zhu, C. Qin, C. Zhang, F. Xu, C.Y. Tan, Y.Y. Jiang, Y.Z. Chen, Nature's contribution to today's pharmacopeia, *Nat. Biotechnol.* 32 (2014) 979–980.
- [35] D.J. Huggins, W. Sherman, B. Tidor, Rational approaches to improving selectivity in drug design, *J. Med. Chem.* 55 (2012) 1424–1444.
- [36] F. Zhu, X.H. Ma, C. Qin, L. Tao, X. Liu, Z. Shi, C.L. Zhang, C.Y. Tan, Y.Z. Chen, Y.Y. Jiang, Drug discovery prospect from untapped species: indications from approved natural product drugs, *PLoS One* 7 (2012) e39782.
- [37] F. Zhu, C.J. Zheng, L.Y. Han, B. Xie, J. Jia, X. Liu, M.T. Tammi, S.Y. Yang, Y.Q. Wei, Y.Z. Chen, Trends in the exploration of anticancer targets and strategies in enhancing the efficacy of drug targeting, *Curr. Mol. Pharmacol.* 1 (2008) 213–232.
- [38] X. Kong, H. Sun, P. Pan, S. Tian, D. Li, Y. Li, T. Hou, Molecular principle of the cyclin-dependent kinase selectivity of 4-(thiazol-5-yl)-2-(phenylamino) pyrimidine-5-carbonitrile derivatives revealed by molecular modeling studies, *Phys. Chem. Chem. Phys.* 18 (2016) 2034–2046.
- [39] C. Brunius, L. Shi, R. Landberg, Large-scale untargeted LC-MS metabolomics data correction using between-batch feature alignment and cluster-based within-batch signal intensity drift correction, *Metabolomics* 12 (2016) 173.
- [40] F. Yang, T. Fu, X. Zhang, J. Hu, W. Xue, G. Zheng, B. Li, Y. Li, X. Yao, F. Zhu, Comparison of computational model and X-ray crystal structure of human serotonin transporter: potential application for the pharmacology of human monoamine transporters, *Mol. Simul.* (2017) 1–10.
- [41] W. Xue, P. Wang, B. Li, Y. Li, X. Xu, F. Yang, X. Yao, Y.Z. Chen, F. Xu, F. Zhu, Identification of the inhibitory mechanism of FDA approved selective serotonin reuptake inhibitors: an insight from molecular dynamics simulation study, *Phys. Chem. Chem. Phys.* 18 (2016) 3260–3271.
- [42] M. Aldeghi, A. Heifetz, M.J. Bodkin, S. Knapp, P.C. Biggin, Predictions of ligand selectivity from absolute binding free energy calculations, *J. Am. Chem. Soc.* 139 (2017) 946–957.
- [43] H. Sun, Y. Li, S. Tian, J. Wang, T. Hou, P-loop conformation governed crizotinib resistance in G2032R-mutated ROS1 tyrosine kinase: clues from free energy landscape, *PLoS Comput. Biol.* 10 (2014) e1003729.
- [44] Y. Yang, Y. Shen, H. Liu, X. Yao, Molecular dynamics simulation and free energy calculation studies of the binding mechanism of allosteric inhibitors with p38alpha MAP kinase, *J. Chem. Inf. Model.* 51 (2011) 3235–3246.
- [45] J. Chen, J. Wang, Q. Zhang, K. Chen, W. Zhu, Probing origin of binding difference of inhibitors to MDM2 and MDMX by polarizable molecular dynamics simulation and QM/MM-GBSA Calculation, *Sci. Rep.* 5 (2015) 17421.
- [46] V. Krishnan, E.J. Nestler, The molecular neurobiology of depression, *Nature* 455 (2008) 894–902.
- [47] B. Maneeton, N. Maneeton, S. Likhitsathian, S. Suttajit, A. Narkpongphun, M. Srisurapanont, P. Woottituk, Comparative efficacy, acceptability, and tolerability of lisdexamfetamine in child and adolescent ADHD: a meta-analysis of randomized, controlled trials, *Drug Des. Devel. Ther.* 9 (2015) 1927–1936.
- [48] L.F. Ward, J.R. Enders, D.S. Bell, H.M. Cramer, F.N. Wallace, G.L. McIntire, Improved chiral separation of methamphetamine enantiomers using CSP-LC-MS-MS, *J. Anal. Toxicol.* 40 (2016) 255–263.
- [49] A. Khan, J. Reinhard, Jr Frederick, Compositions and Methods for Treating Depression, ADHD and Other Central Nervous System Disorders Employing Novel Bupropion Compounds, and Methods for Production and Use of Novel Bupropion Compounds and Formulations, WO2012118562A1 (2012).
- [50] N. Benson, N. Snelder, B. Ploeger, C. Napier, H. Sale, N.J. Birdsall, R.P. Butt, P.H. van der Graaf, Estimation of binding rate constants using a simultaneous mixed-effects method: application to monoamine transporter reuptake inhibitor roboxetine, *Br. J. Pharmacol.* 160 (2010) 389–398.
- [51] C.D. Bereder, B. MD., Method of Treatment of Depression, US2012115871A1 (2012).
- [52] M.A. Larkin, G. Blackshields, N.P. Brown, R. Chenna, P.A. McGettigan, H. McWilliam, F. Valentin, I.M. Wallace, A. Wilm, R. Lopez, J.D. Thompson,

- T.J. Gibson, D.G. Higgins, Clustal W and Clustal X version 2.0, *Bioinformatics* 23 (2007) 2947–2948.
- [53] B. Webb, A. Sali, Comparative protein structure modeling using MODELLER, *Curr. Protoc. Protein Sci.* 86 (2016) 1–37 (2. 9).
- [54] Glide v. 5.5, Schrödinger, LLC, New York, NY, 2009.
- [55] K. Arnold, L. Bordoli, J. Kopp, T. Schwede, The SWISS-MODEL workspace: a web-based environment for protein structure homology modelling, *Bioinformatics* 22 (2006) 195–201.
- [56] SYBYL X Molecular Modeling Software v. 1.2, Tripos Associates, St. Louis, Missouri, USA, 2011.
- [57] L. Guo, J. Wang, S. Qian, X. Yan, R. Chen, G. Meng, Construction and structural modeling of a single-chain Fv-asparaginase fusion protein resistant to proteolysis, *Biotechnol. Bioeng.* 70 (2000) 456–463.
- [58] A. Nayeem, D. Sitkoff, S. Krystek Jr., A comparative study of available software for high-accuracy homology modeling: from sequence alignments to structural models, *Protein Sci.* 15 (2006) 808–824.
- [59] S. Reddy Ch, K. Vijayasathya, E. Srinivas, G.M. Sastry, G.N. Sastry, Homology modeling of membrane proteins: a critical assessment, *Comput. Biol. Chem.* 30 (2006) 120–126.
- [60] B. Webb, A. Sali, Comparative protein structure modeling using MODELLER, *Curr. Protoc. Bioinformatics* 47 (2014) 1–32 (5. 6).
- [61] M. Sund-Levander, E. Grodzinsky, Assessment of body temperature measurement options, *Br. J. Nurs.* 942 (2013) 944–950 (22).
- [62] R.A. Laskowski, M.W. MacArthur, D.S. Moss, J.M. Thornton, PROCHECK_a program to check the stereochemical quality of protein structures, *J. Appl. Crystallogr.* 26 (1993) 283–291.
- [63] P. Wang, F. Yang, H. Yang, X. Xu, D. Liu, W. Xue, F. Zhu, Identification of dual active agents targeting 5-HT1A and SERT by combinatorial virtual screening methods, *Biomed. Mater. Eng.* 26 (Suppl. 1) (2015) S2233–2239.
- [64] A. Abdolmaleki, F. Ghasemi, J.B. Ghasemi, Computer-aided drug design to explore cycloextrin therapeutics and biomedical applications, *Chem. Biol. Drug Des.* 89 (2017) 257–268.
- [65] M. Hernandez-Rodriguez, M.C. Rosales-Hernandez, J.E. Mendieta-Wejbe, M. Martinez-Archundia, J.C. Basurto, Current tools and methods in molecular dynamics (MD) simulations for drug design, *Curr. Med. Chem.* 23 (2016) 3909–3924.
- [66] E.L. Wu, X. Cheng, S. Jo, H. Rui, K.C. Song, E.M. Davila-Contreras, Y. Qi, J. Lee, V. Monje-Galvan, R.M. Venable, J.B. Klauda, W. Im, CHARMM-GUI membrane builder toward realistic biological membrane simulations, *J. Comput. Chem.* 35 (2014) 1997–2004.
- [67] V. Hornak, R. Abel, A. Okur, B. Strockbine, A. Roitberg, C. Simmerling, Comparison of multiple Amber force fields and development of improved protein backbone parameters, *Proteins* 65 (2006) 712–725.
- [68] AMBER v. 14, AMBER, University of California, San Francisco, 2014.
- [69] J.A. Maier, C. Martinez, K. Kasavajhala, L. Wickstrom, K.E. Hauser, C. Simmerling, ff14SB: improving the accuracy of protein side chain and backbone parameters from ff99SB, *J. Chem. Theory Comput.* 11 (2015) 3696–3713.
- [70] C.J. Dickson, B.D. Madej, A.A. Skjevik, R.M. Betz, K. Teigen, I.R. Gould, R.C. Walker, Lipid14: the Amber lipid force field, *J. Chem. Theory Comput.* 10 (2014) 865–879.
- [71] G. Zheng, W. Xue, P. Wang, F. Yang, B. Li, X. Li, Y. Li, X. Yao, F. Zhu, Exploring the inhibitory mechanism of approved selective norepinephrine reuptake inhibitors and reboxetine enantiomers by molecular dynamics study, *Sci. Rep.* 6 (2016) 26883.
- [72] Y. Hara, S. Murayama, Effects of analgesic-antipyretics on the spinal reflex potentials in cats: an analysis of the excitatory action of aminopyrine, *Nihon Yakurigaku Zasshi* 100 (1992) 383–390.
- [73] M. Springborg, B. Kirtman, Efficient vector potential method for calculating electronic and nuclear response of infinite periodic systems to finite electric fields, *J. Chem. Phys.* 126 (2007) 104107.
- [74] I. Massova, P.A. Kollman, Combined molecular mechanical and continuum solvent approach (MM-PBSA_GBSA) to predict ligand, *Perspect. Drug Discovery Des.* 18 (2000) 113–135.
- [75] L. Xu, H. Sun, Y. Li, J. Wang, T. Hou, Assessing the performance of MM/PBSA and MM/GBSA methods. 3. The impact of force fields and ligand charge models, *J. Phys. Chem. B* 117 (2013) 8408–8421.
- [76] H. Sun, Y. Li, M. Shen, S. Tian, L. Xu, P. Pan, Y. Guan, T. Hou, Assessing the performance of MM/PBSA and MM/GBSA methods. 5. Improved docking performance using high solute dielectric constant MM/GBSA and MM/PBSA rescoring, *Phys. Chem. Chem. Phys.* 16 (2014) 22035–22045.
- [77] F. Chen, H. Liu, H. Sun, P. Pan, Y. Li, D. Li, T. Hou, Assessing the performance of the MM/PBSA and MM/GBSA methods. 6. Capability to predict protein-protein binding free energies and re-rank binding poses generated by protein-protein docking, *Phys. Chem. Chem. Phys.* 18 (2016) 22129–22139.
- [78] G.G. Froesner, D.A. Peterson, F.W. Deinhardt, A.W. Holmes, Transmission of hepatitis A and hepatitis B by shared needle, *Lancet* 1 (1973) 1183.
- [79] W. Jörg, P.S. Shenkin, W. Clark Still, Approximate atomic surfaces from linear combinations of pairwise overlaps (LCPO), *J. Comput. Chem.* 20 (1999) 217–230.
- [80] H. Sun, Y. Li, D. Li, T. Hou, Insight into crizotinib resistance mechanisms caused by three mutations in ALK tyrosine kinase using free energy calculation approaches, *J. Chem. Inf. Model.* 53 (2013) 2376–2389.
- [81] H. Koldso, H.E. Autzen, J. Grouleff, B. Schiott, Ligand induced conformational changes of the human serotonin transporter revealed by molecular dynamics simulations, *PLoS One* 8 (2013) e63635.
- [82] S. Tippmann, Programming tools: adventures with R, *Nature* 517 (2015) 109–110.
- [83] F. Zhu, C. Qin, L. Tao, X. Liu, Z. Shi, X. Ma, J. Jia, Y. Tan, C. Cui, J. Lin, C. Tan, Y. Jiang, Y. Chen, Clustered patterns of species origins of nature-derived drugs and clues for future bioprospecting, *Proc. Natl. Acad. Sci. U. S. A.* 108 (2011) 12943–12948.
- [84] G.J. Szekely, M.L. Rizzo, Hierarchical clustering via joint between-within distances extending Ward's minimum variance method, *J. Classif.* 22 (2005) 151–183.
- [85] I. Letunic, P. Bork, Interactive tree of life (iTOL): an online tool for phylogenetic tree display and annotation, *Bioinformatics* 23 (2007) 127–128.
- [86] V. Hooda, P.B. Gundala, P. Chinthala, Sequence analysis and homology modeling of peroxidase from *Medicago sativa*, *Bioinformation* 8 (2012) 974–979.
- [87] R.L. Williard, L.D. Middaugh, H.J. Zhu, K.S. Patrick, Methylphenidate and its ethanol transesterification metabolite ethylphenidate: brain disposition, monoamine transporters and motor activity, *Behav. Pharmacol.* 18 (2007) 39–51.
- [88] L.D. Simmler, T.A. Buser, M. Donzelli, Y. Schramm, L.H. Dieu, J. Huwyler, S. Chaboz, M.C. Hoener, M.E. Liechti, Pharmacological characterization of designer cathinones in vitro, *Br. J. Pharmacol.* 168 (2013) 458–470.
- [89] M. Rutkowski, M. Draminski, Phosphorylation of acylonucleosides by nucleoside phosphotransferase from higher plants and bacteria, *Acta Biochim. Pol.* 38 (1991) 449–457.
- [90] F.I. Carroll, B.E. Blough, P. Abraham, A.C. Mills, J.A. Holleman, S.A. Wolckenhauer, A.M. Decker, A. Landavazo, K.T. McElroy, H.A. Navarro, M.B. Gatch, M.J. Forster, Synthesis and biological evaluation of bupropion analogues as potential pharmacotherapies for cocaine addiction, *J. Med. Chem.* 52 (2009) 6768–6781.
- [91] F.P. Bymaster, J.S. Katner, D.L. Nelson, S.K. Hemrick-Luecke, P.G. Threlkeld, J.H. Heiligenstein, S.M. Morin, D.R. Gehlert, K.W. Perry, Atomoxetine increases extracellular levels of norepinephrine and dopamine in prefrontal cortex of rat: a potential mechanism for efficacy in attention deficit/hyperactivity disorder, *Neuropsychopharmacology* 27 (2002) 699–711.
- [92] M. Tatsumi, K. Groshan, R.D. Blakely, E. Richelson, Pharmacological profile of antidepressants and related compounds at human monoamine transporters, *Eur. J. Pharmacol.* 340 (1997) 249–258.
- [93] T.M. Oakes, M.A. Dellva, K. Waterman, M. Greenbaum, C. Poppe, C. Goldberger, J. Ahl, D.G. Perahia, Edvoxetine compared to placebo as adjunctive therapy to selective serotonin reuptake inhibitors in the prevention of symptom re-emergence in major depressive disorder, *Curr. Med. Res. Opin.* 31 (2015) 1179–1189.
- [94] F. Zeng, J. Mun, N. Jarkas, J.S. Stehouwer, R.J. Voll, G.D. Tamagnan, L. Howell, J.R. Votaw, C.D. Kilts, C.B. Nemeroff, M.M. Goodman, Synthesis, radiosynthesis, and biological evaluation of carbon-11 and fluorine-18 labeled reboxetine analogues: potential positron emission tomography radioligands for in vivo imaging of the norepinephrine transporter, *J. Med. Chem.* 52 (2009) 62–73.
- [95] C.M. Reyes, P.A. Kollman, Structure and thermodynamics of RNA-protein binding: using molecular dynamics and free energy analyses to calculate the free energies of binding and conformational change, *J. Mol. Biol.* 297 (2000) 1145–1158.
- [96] T. Hou, J. Wang, Y. Li, W. Wang, Assessing the performance of the MM/PBSA and MM/GBSA methods. 1. The accuracy of binding free energy calculations based on molecular dynamics simulations, *J. Chem. Inf. Model.* 51 (2011) 69–82.
- [97] S. Genheden, U. Ryde, The MM/PBSA and MM/GBSA methods to estimate ligand-binding affinities, *Expert Opin. Drug Discovery* 10 (2015) 449–461.
- [98] K.C. Schmitt, M.E. Reith, The atypical stimulant and nootropic modafinil interacts with the dopamine transporter in a different manner than classical cocaine-like inhibitors, *PLoS One* 6 (2011) e25790.
- [99] L. Sorensen, J. Andersen, M. Thomsen, S.M. Hansen, X. Zhao, A. Sandelin, K. Stromgaard, A.S. Kristensen, Interaction of antidepressants with the serotonin and norepinephrine transporters: mutational studies of the S1 substrate binding pocket, *J. Biol. Chem.* 287 (2012) 43694–43707.
- [100] K.C. Schmitt, S. Mamidyalala, S. Biswas, A.K. Dutta, M.E. Reith, Bivalent phenethylamines as novel dopamine transporter inhibitors: evidence for multiple substrate-binding sites in a single transporter, *J. Neurochem.* 112 (2010) 1605–1618.
- [101] C.S. Vasavi, R. Tamizhselvi, P. Munusami, Drug resistance mechanism of L10F, L10F/N88S and L90M mutations in CRF01_AE HIV-1 protease: molecular dynamics simulations and binding free energy calculations, *J. Mol. Graph. Model.* 75 (2017) 390–402.
- [102] K.K. Skeby, J. Sorensen, B. Schiott, Identification of a common binding mode for imaging agents to amyloid fibrils from molecular dynamics simulations, *J. Am. Chem. Soc.* 135 (2013) 15114–15128.
- [103] H. Koldso, A.B. Christiansen, S. Sinning, B. Schiott, Comparative modeling of the human monoamine transporters: similarities in substrate binding, *ACS Chem. Neurosci.* 4 (2013) 295–309.
- [104] A. Seddik, M. Holy, R. Weissensteiner, B. Zdrzil, H.H. Sitte, G.F. Ecker, Probing the selectivity of monoamine transporter substrates by means of molecular modeling, *Mol. Inf.* 32 (2013) 409–413.
- [105] J. Zhou, Norepinephrine transporter inhibitors and their therapeutic potential, *Drugs Future* 29 (2004) 1235–1244.
- [106] K. Severinsen, J.F. Kraft, H. Koldso, K.A. Vinberg, R.B. Rothman, J.S. Partilla, O. Wiborg, B. Blough, B. Schiott, S. Sinning, Binding of the amphetamine-like 1-phenyl-piperazine to monoamine transporters, *ACS Chem. Neurosci.* 3 (2012) 693–705.